

Article

# K<sub>2</sub>O Doped Dolomite as Heterogeneous Catalyst for Fatty Acid Methyl Ester Production from Palm Oil

Muhammad Yahaya <sup>1,2</sup>, Irmawati Ramli <sup>1,3,\*</sup> , Ernee Noryana Muhamad <sup>1,3</sup>,  
Nor Shafizah Ishak <sup>1,3</sup>, Usman Idris Nda-Umar <sup>1,3</sup> and Yun Hin Taufiq-Yap <sup>1,3</sup>

<sup>1</sup> Department of Chemistry, Faculty of Science Universiti Putra Malaysia, Serdang 43400 UPM, Selangor Darul Ehsan, Malaysia; koljiya@yahoo.com (M.Y.); ernee@upm.edu.my (E.N.M.); norshafizah@gmail.com (N.S.I.); uindaumar@gmail.com (U.I.N.-U.); taufiq@upm.edu.my (Y.H.T.-Y.)

<sup>2</sup> Desert Research Monitoring and Control Centre, Yobe State University, 620253 KM7, Gujba Road, Damaturu P. M. B 1144, Yobe State, Nigeria

<sup>3</sup> Catalysis Science and Technology Research Centre (PutraCat), Faculty of Science Universiti Putra Malaysia, Serdang 43400 UPM, Selangor Darul Ehsan, Malaysia

\* Correspondence: irmawati@upm.edu.my

Received: 16 May 2020; Accepted: 1 June 2020; Published: 16 July 2020



**Abstract:** Biodiesel obtained from palm oil over an environmentally friendly catalyst is highly desirable. For that matter, dolomite, a natural material was used as a catalyst in this work, and this included potassium oxide (K<sub>2</sub>O)-doped dolomite, 5 wt% K/D, 10 wt% K/D, 15 wt% K/D, and 20 wt% K/D. X-ray diffraction analysis of dolomite revealed the CaO and MgO phases with high crystallinity, in which intensity reduced after doped with varying concentrations of K<sub>2</sub>O. When the catalysts were evaluated, the K<sub>2</sub>O-doped dolomite exhibited a better catalytic activity for palm oil transesterification. In the presence of K<sub>2</sub>O, the methyl ester reached 98.7%, with the highest being displayed by 15 wt% K/D as compared to 87% over dolomite at reaction temperature of 60 °C, 12:1 methanol to palm oil ratio, 1 wt% catalyst amount and 1 h reaction time. SEM revealed that as more K<sub>2</sub>O was doped on dolomite, the particles became more agglomerated, with a reduced BET surface area of 1.3 m<sup>2</sup>/g in 20 wt% K/D as opposed to homogeneously small-sized MgO and CaO particles in dolomite with a high BET surface area of 19.0 m<sup>2</sup>/g. However, the high activity of the doped catalyst was dictated by the high amount of basic site, as evidenced in TPD-CO<sub>2</sub> which showed an increase in the capacity of the basic site with an increased amount of K<sub>2</sub>O. The catalyst was also reusable up to six times with a negligible decrease in activity due to K<sup>+</sup> leaching.

**Keywords:** dolomite; K<sub>2</sub>O/dolomite; biodiesel; transesterification; palm oil

## 1. Introduction

The rise in energy demand and price, environmental concerns and fossil fuel depletion have triggered the search for an alternative energy source that is renewable [1]. In this respect, due attention is given to biodiesel due to its numerous merits over petroleum-based fuel [2]. Owing to its biodegradability, negligible toxicity, renewability, low carbon emission, and no or little engine modification when used as fuel, biodiesel has been selected as the promising fuel [2–5]. Conventionally, biodiesel can be obtained via a reaction of triglyceride of vegetable oil or animal fats with the low chain alcohol, preferably methanol with the aid of catalyst (acid or base) through a process known as transesterification reaction [6,7]. Though, it was revealed that the transesterification reaction using a basic homogeneous catalyst is 4000 times faster than acid homogeneous catalyst [8,9]. Nonetheless, the reaction showed numerous weaknesses, which include generating a colossal volume of wastewater,

being unable to recover and reuse a catalyst, causing corrosion in reactors and a decrease in FAME yield [10,11]. To circumvent difficulties related with the use of homogeneous catalysts, researchers have suggested the use of heterogeneous catalysts [12]. The benefits of the heterogeneous catalyst over a conventional homogeneous catalyst include easy separation from the product, regenerability, reusability and negligible toxicity [13]. Various numbers of heterogeneous catalysts have been used for the production of biodiesel. For example, a metal single-base oxide such as calcium oxide (CaO), magnesium oxide (MgO) and strontium oxide [14]. Furthermore, the heterogeneous base catalyst is further categorized into solid alkali catalyst and base catalyst support. The catalyst exhibits a low catalytic activity per unit mass because the surface area is the only contact area between the triglyceride substrate and the catalyst. After introducing the active ingredient on the parent material with a large surface area, this served as an alternative source in reducing the amount of catalyst needed to obtain a similar level of catalytic activity [15]. However, the catalyst support is also used to reduce the mass transfer limitation for solid catalyst during the transesterification reaction [16]. To date, only a small number among them (catalyst) are employed on a large scale as a result of catalyst processing costs. To overcome these drawbacks, several researchers concentrated on natural sources or solid waste as materials for catalyst preparation. Clays from natural source materials which include bentonite [1], hydrotalcite [17], palygorskite [18], and sepiolite [19], are found in excess. Their availability, inexpensive and environmentally friendly nature qualified them to be used as catalyst for biodiesel production. Dolomite is one of the catalysts used in biodiesel production which is available and inexpensive with negligible toxicity. It occurs naturally with high basic strength and a reasonable surface area [20,21]. Chemically, dolomite is made up of carbonate of magnesium and calcium and a small amount of other compounds [22]. Dolomite can be decomposed into two phases:

1. At the initial phase, the breaking down and formation of  $\text{MgCO}_3$  and  $\text{MgO}$ , respectively, occur at a temperature range of 350–545 °C [23];
2. At the subsequent phase, at 850 °C,  $\text{CaCO}_3$  decomposes and  $\text{CaO}$  is formed [24].

The consequential yield of dolomite after decomposition is  $\text{CaO}$  and  $\text{MgO}$ . It can be presented in Equation (1).



The natural dolomite (Figure 1) is made up of analog layers of  $\text{Mg}(\text{CO}_3)$ - $\text{Ca}(\text{CO}_3)$  and has a structural similarity to calcite ( $\text{CaCO}_3$ ). Similarly, minerals such as dolomitic rocks also have a phase of Ca-rich magnesium calcite ( $\text{Mg}_x\text{Ca}_{1-x}\text{CO}_3$ ) which agrees with a different layered structure in the case of  $\text{Ca}(\text{CO}_3)$  and mixed  $\text{Mg}(\text{CO}_3)$ - $\text{Ca}(\text{CO}_3)$  [25].

It was reported that solid base catalyst exhibits maximum catalytic activity, however, a high reaction temperature and longer reaction time are needed before achieving high conversion. [26] investigated the catalytic activity of soybean oil with  $\text{MgO}$  as a solid base catalyst; it needed a reaction temperature of 250 °C before a 99% yield was achieved. Similarly, [27] studied the catalytic activity of potassium iodide supported on alumina as a heterogeneous base catalyst for the transesterification reaction of soybean to methyl ester. A total of 96% of biodiesel was achieved after 8 h reaction time. To improve FAME yield at mild reaction conditions, the various literature have reported the use of  $\text{K}_2\text{CO}_3$  as a solid basic active component that can be used to impregnate different catalyst supports [28,29]. The aim of this research is to increase the effectiveness of dolomite by impregnating with potassium oxide ( $\text{K}_2\text{O}$ ) and to produce methyl ester under mild reaction conditions. Following a detailed literature search, no report on incorporating  $\text{K}_2\text{O}$  with dolomite as a catalyst in transesterification reaction that produces biodiesel. The physicochemical properties of the prepared catalyst were carried out using XRD, BET, TPD- $\text{CO}_2$ , TGA, SEM and FTIR. The catalytic stability was investigated to evaluate the reusability and lixiviate of the catalyst.

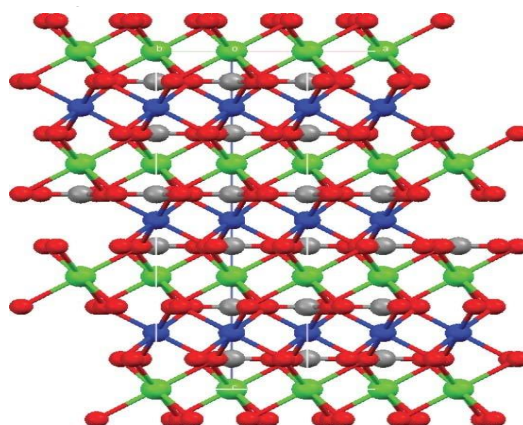


**Figure 1.** Structure of dolomite  $\text{MgCa}(\text{CO}_3)_2$  C-grey,  $\text{Mg}^{2+}$ -blue,  $\text{Ca}^{2+}$ -green,  $\text{O}^{2-}$ -red.

### Mechanism of $\text{K}_2\text{O}/\text{CaO}-\text{MgO}$ Catalyst

The reaction mechanism of the catalyst is shown in Figure 2. The initial stage of the mechanism involves the removal of a proton ( $\text{H}^+$ ) from the water molecule ( $\text{H}_2\text{O}$ ) to form the surface  $\text{OH}^-$  on the basic site. In the second stage, methoxide ion and water are produced after  $\text{H}^+$  is removed from methanol. In the third stage, the methanol can adsorb on  $\text{K}_2\text{O}/\text{CaO}-\text{MgO}$  separately. The fourth stage involves the formation of an intermediate due to an attack from the methoxide ion to glycerol molecule, which is subsequently protonated. The tetrahedral can further react with methanol to produce methoxide ion. In the last stage, the methyl ester and acyl glycerol or glycerol is formed as a result of rearrangements of a tetrahedral intermediate. Adaptation from [30] with modification.

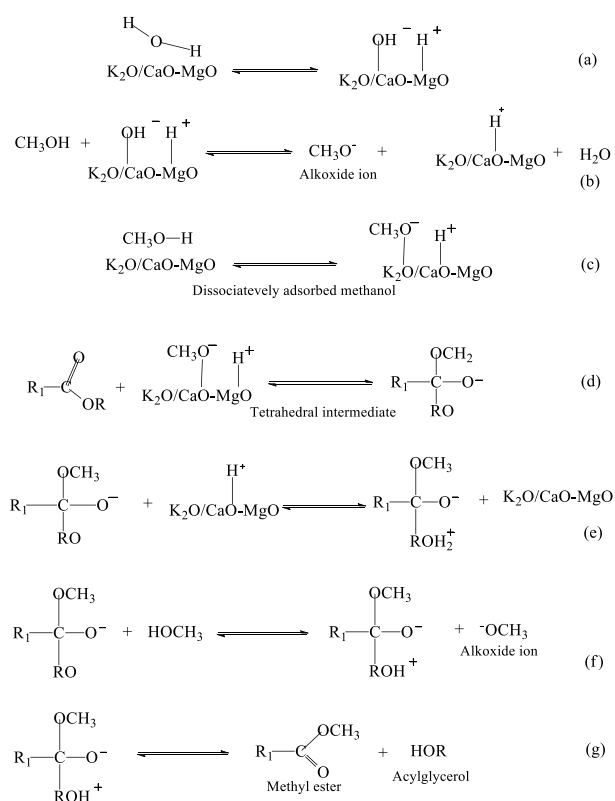


**Figure 2.** Mechanism of solid base catalyst (a) Surface  $\text{OH}^-$  formed on  $\text{K}_2\text{O}/\text{CaO}-\text{MgO}$  (b)  $\text{CH}_3\text{O}^-$  and  $\text{H}_2\text{O}$  formed (c)  $\text{CH}_3\text{OH}$  adsorb separately on  $\text{K}_2\text{O}/\text{CaO}-\text{MgO}$  (d) Intermediate formed (e) Intermediate subsequently protonated (f) Intermediate react with methanol (g) Rearrangement of tetrahedral result in the formation of methyl ester and glycerol [30].

## 2. Results

### 2.1. X-ray Diffraction Analysis (XRD)

The XRD patterns of dolomite and  $K_2O$ -doped dolomite catalysts are depicted in Figure 3. Dolomite exhibited peaks at  $2\theta = 32.4^\circ$ ,  $37.6^\circ$ ,  $54.2^\circ$ ,  $64.6^\circ$ ,  $67.9^\circ$  (JCPDS = 01-074-1226) which is attributed to quicklime (CaO) and at  $2\theta = 43.5^\circ$  and  $62^\circ$  (JCPDS = 01-075-1525) ascribed to periclase (MgO) with cubic as their crystal structure. Similar results were revealed by [20,22]. The intense peaks appeared in the calcined dolomite, suggesting a high crystallinity of both compounds. Earlier, researchers have concentrated on the production of biodiesel through individual quicklime and periclase (CaO and MgO), as they increase the basic active site for methyl ester production [25]. When  $K_2O$  was introduced onto dolomite, the reflection of CaO and MgO of the doped catalysts (5 wt% K/D, 10 wt% K/D, 15 wt% K/D and 20 wt% K/D) was reduced and a new peak of  $K_2O$  appeared at  $2\theta = 33.1^\circ$  (JCPDS: 00-025-0626), which can be seen in Figure 3b–e). The CaO peak at  $2\theta = 32.4^\circ$  shifted slightly, as in the case for 5 wt% K/D, 10 wt% K/D, and 15 wt% K/D Figure 3b–d) to  $2\theta = 31.5^\circ$ . This slight shift could be due to a well-preserved CaO crystal structure [18]. Other peaks appeared at  $2\theta = 53.8^\circ$  (JCPDS: 00-008-0479) which is attributed to  $Mg(OH)_2$  and at  $2\theta = 30.2^\circ$  (JCPDS: 01-087-1863) which is assigned to  $Ca(OH)_2$  with rhombohedral as their crystal structure. However, these peaks were not pronounced on 20 wt% K/D catalyst. The formation of these new phases may be due to the exposure to moisture of MgO and CaO to form  $Mg(OH)_2$  and  $Ca(OH)_2$  respectively.

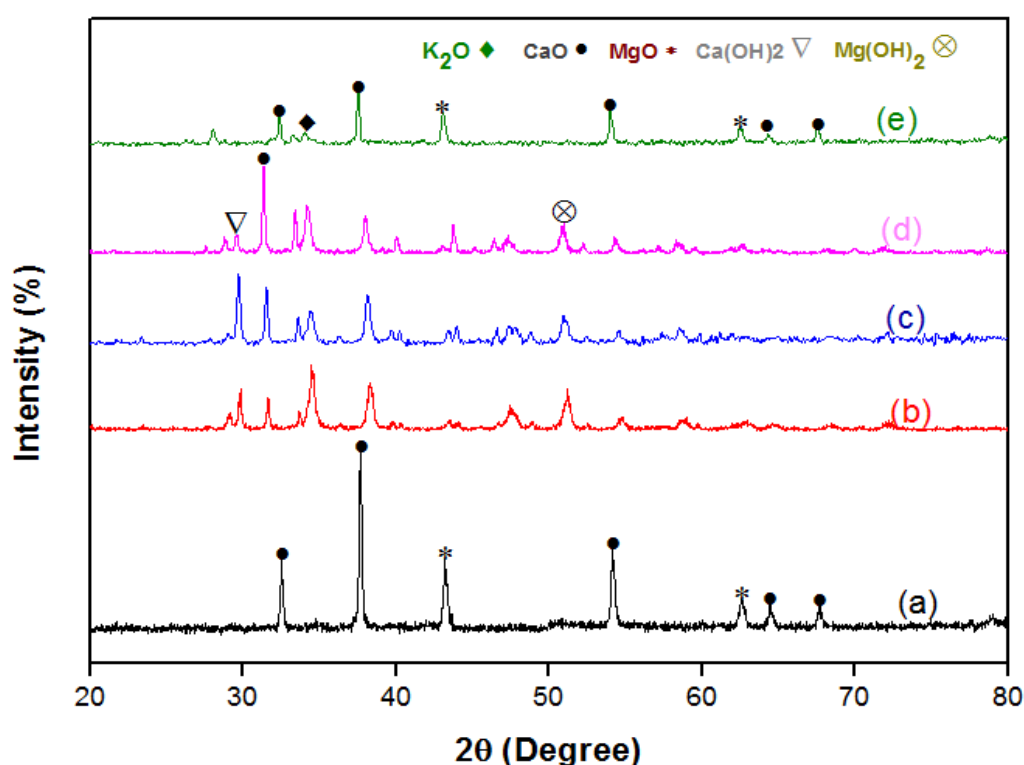
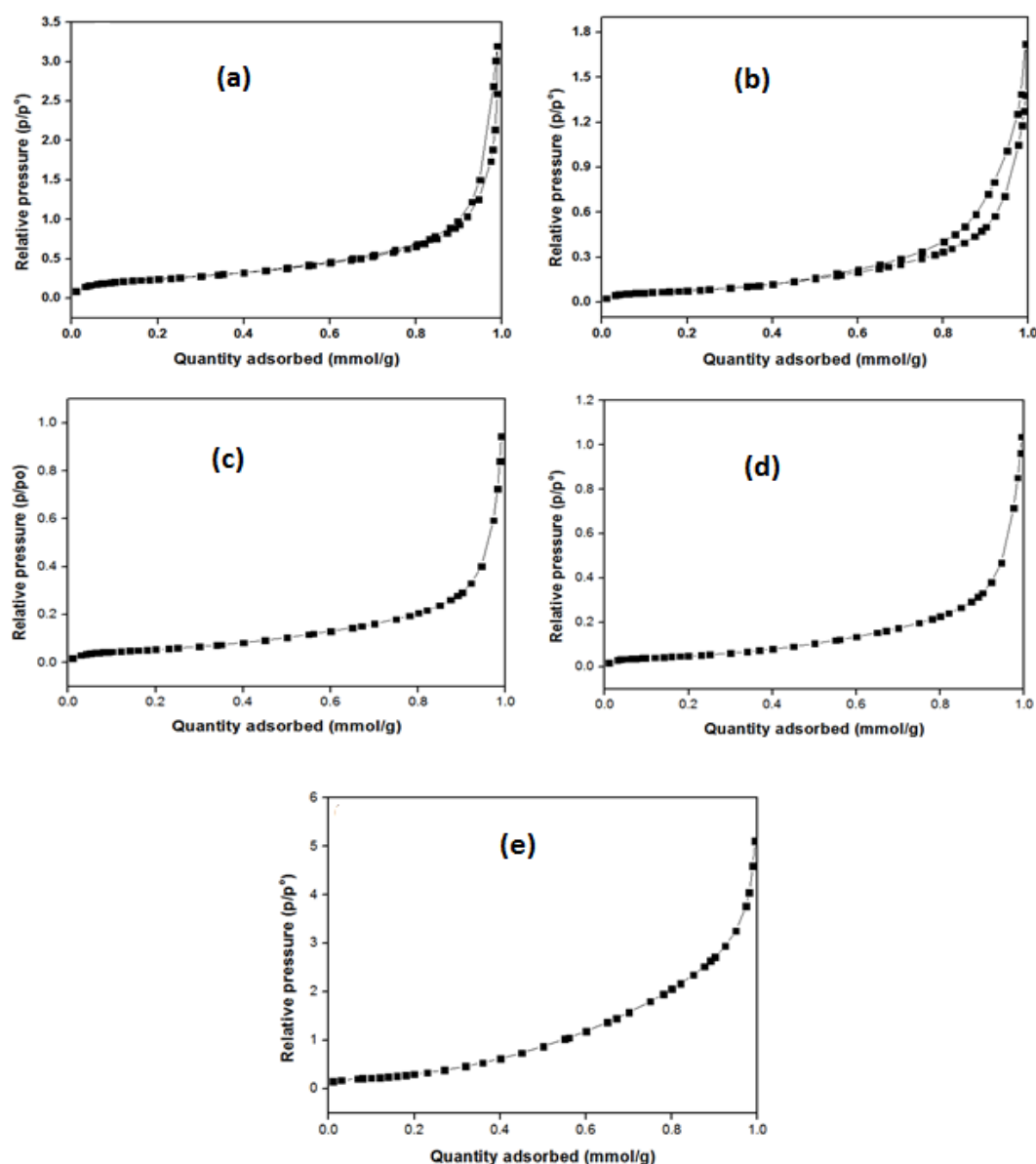


Figure 3. XRD pattern of (a) Dolomite (b) 5 wt% K/D (c) 10 wt% K/D (d) 15 wt% K/D (e) 20 wt% K/D.

### 2.2. Brunauer-Emmett-Teller Surface Area Measurement (BET)

The BET surface area, pore volume and average pore diameter of dolomite and  $K_2O$ -doped dolomite are seen in Table 1. The BET surface area of the obtained dolomite was  $19.0 \text{ m}^2/\text{g}$ , which is higher than the BET surface area of dolomite ( $14.8 \text{ m}^2/\text{g}$ ) reported by [22] under a similar calcination temperature. According to [20], it is expected that after the calcination of dolomite, the compounds ( $CaMg(CO_3)_2$ ) transform into CaO and MgO and create pores which will enhance the surface area.

The BET surface area of dolomite was also found to be higher than that of the synthesized  $K_2O$ -doped dolomite which was between 1.3 to 6.9  $m^2/g$ . It was observed that the BET surface area of synthesized  $K_2O$ -doped dolomite decreases as the concentration of  $K_2O$  increases in the catalyst support (dolomite) from 5, 10, 15 and 20 wt%; this observation was anticipated and synchronized with pore volume. Furthermore, after incorporating  $K_2O$  onto dolomite, the  $K_2O$  covers the surface of dolomite and eventually blocks the pores which are responsible for the decrease in the BET surface area. A similar observation was reported by Shan and his co-workers, they discovered the BET surface area of a natural mineral (palygorskite) to be 178.7  $m^2/g$ . The BET surface area was then reduced to 8.8  $m^2/g$  after being incorporated with  $K_2O$  [18]. Based on IUPAC identification, the catalysts in Figure 4a,b) revealed type IV adsorption isotherm with type H1 hysteresis. The catalyst in Figure 4c–e) revealed type II adsorption isotherm with a type H4 hysteresis loop. The hysteresis loop is the main characteristic feature of type IV adsorption isotherm, which is related to the capillary condensation of the adsorbate. The differential volumes of the catalyst and the support were depicted in Figure 5. This shows all the catalysts and the supports within the mesoporous region (2–50 nm) [31].



**Figure 4.** Adsorption-desorption isotherm for (a) Dolomite (b) 5 wt% K/D (c) 10 wt% K/D (d) 15 wt% K/D. (e) 20 wt% K/D.

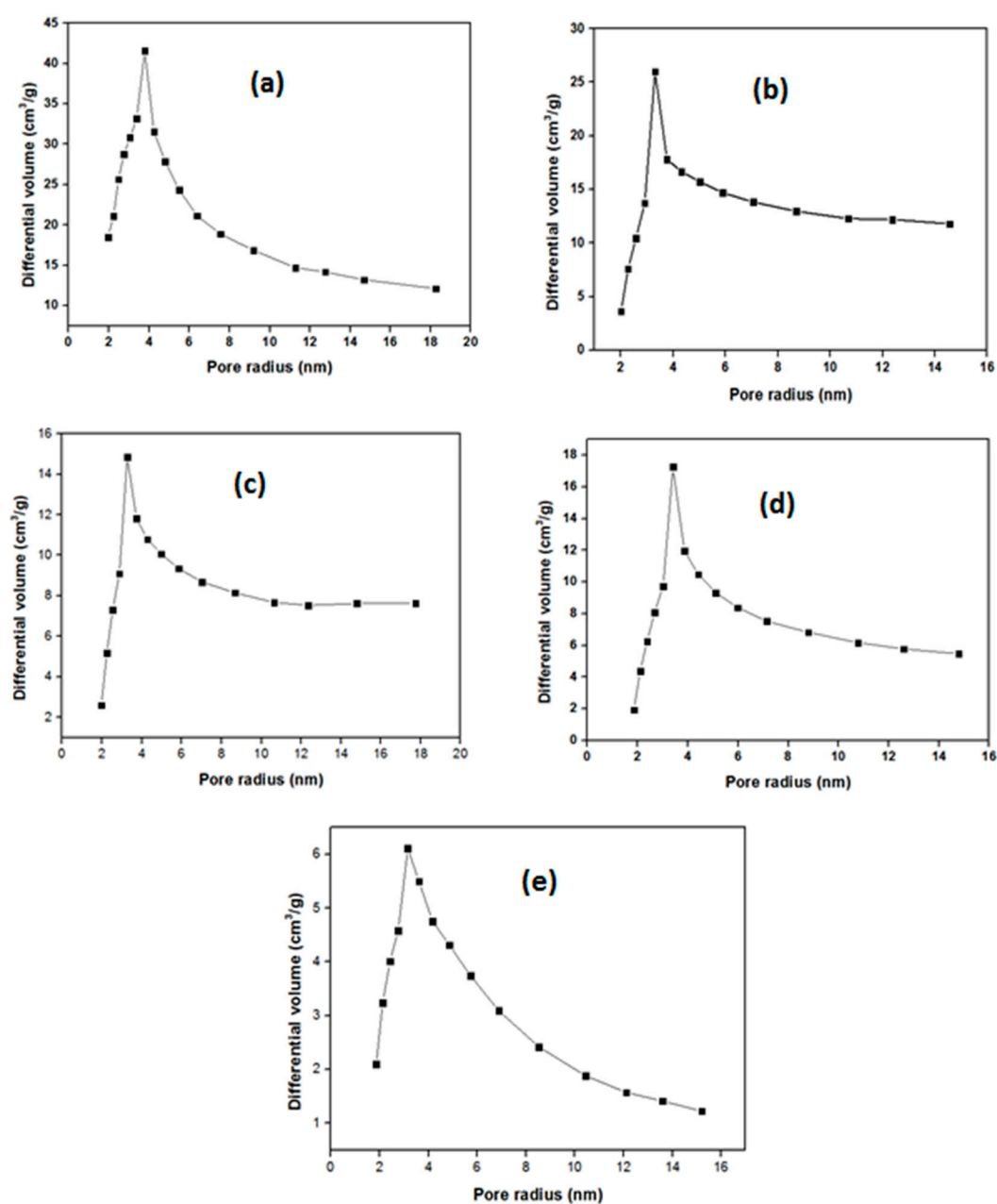


Figure 5. Pore size distribution of (a) Dolomite (b) 5 wt% K/D (c) 10 wt% K/D (d) 15 wt% K/D (e) 20 wt% K/D.

Table 1. Textual properties.

Catalyst	BET Surface Area (m <sup>2</sup> /g)	Pore Volume (cc/g)	Pore Size (Å)
Dolomite	19.0	0.034	57.16
5 wt% K/D	6.9	0.024	60.54
10 wt% K/D	5.2	0.019	60.02
15 wt% K/D	4.2	0.015	61.24
20 wt% K/D	1.3	0.008	55.56

### 2.3. Temperature Programmed Desorption (TPD-CO<sub>2</sub>)

To study the basicity of the dolomite and K<sub>2</sub>O/dolomite catalysts, the compounds were subjected to TPD-CO<sub>2</sub> and the results were plotted in Figure 6. The peaks of all samples followed a similar trajectory, confirming that the doping of K<sub>2</sub>O did not disrupt the dolomite's CaO and MgO structure.

It was reported that the CO<sub>2</sub> desorption peak appeared at a temperature of ~250 °C, which is ascribed to the interaction in the catalyst between CO<sub>2</sub> and the weak basic site [32], whereas the appearance of a peak at a temperature between 250–550 °C can be ascribed to the interaction of CO<sub>2</sub> and a moderate basic site. Furthermore, the appearance of the desorption peak at extremely high temperatures (>550 °C) was a result of the strong basic site [33,34]. The spectrum revealed that dolomite and varied K<sub>2</sub>O/dolomite show peaks and a well-defined desorption band at a region of 550–800 °C, which can be ascribed to strong basic sites in the catalyst with a strong interaction of CO<sub>2</sub>. Dolomite exhibited 501.4 μmol/g as the amount of CO<sub>2</sub> desorbed, which is quite low when compared with 5, 10, 15, and 20 wt% K<sub>2</sub>O/dolomite compounds, which exhibited 892.2, 1692.2, 3165.2 and 2835.15 μmol/g, respectively (Table 2). It was deduced that the amount of CO<sub>2</sub> desorbed increased linearly when the concentration of dopant increased from 5 to 15 wt%. For dolomite, overlapped peaks maxima are observed at 601 and 621 °C as a result of two rapid desorptions of CO<sub>2</sub> from the surface of two metal oxide phases (MgO and CaO). When K<sub>2</sub>O was added, a third desorption peak appears at a much higher temperature, suggesting the presence of additional basic sites of the doped catalyst. Furthermore, the high dosage of K<sub>2</sub>O contributes to the remarkable increase in total basic sites due to the synergic effect between K<sub>2</sub>O, MgO and CaO [33]. However, when the concentration of dopant increases to 20 wt%, a substantial decrease in the capacity of the basic site was observed. This is as a result of the saturation of K<sub>2</sub>O as evidence in a single desorption peak on the surface of dolomite that resulted in an incessant agglomeration of K<sub>2</sub>O on the surface, as can be proved by SEM image, which causes a change in the structural properties, as electron transfer between the K<sub>2</sub>O and dolomite becomes difficult by the agglomerated phase. This will affect the active phase of K<sub>2</sub>O/dolomite and subsequently decrease the capacity of the basic site [35]. The desorption temperature of all the samples corroborated with the decomposition temperature revealed by TGA-DTG

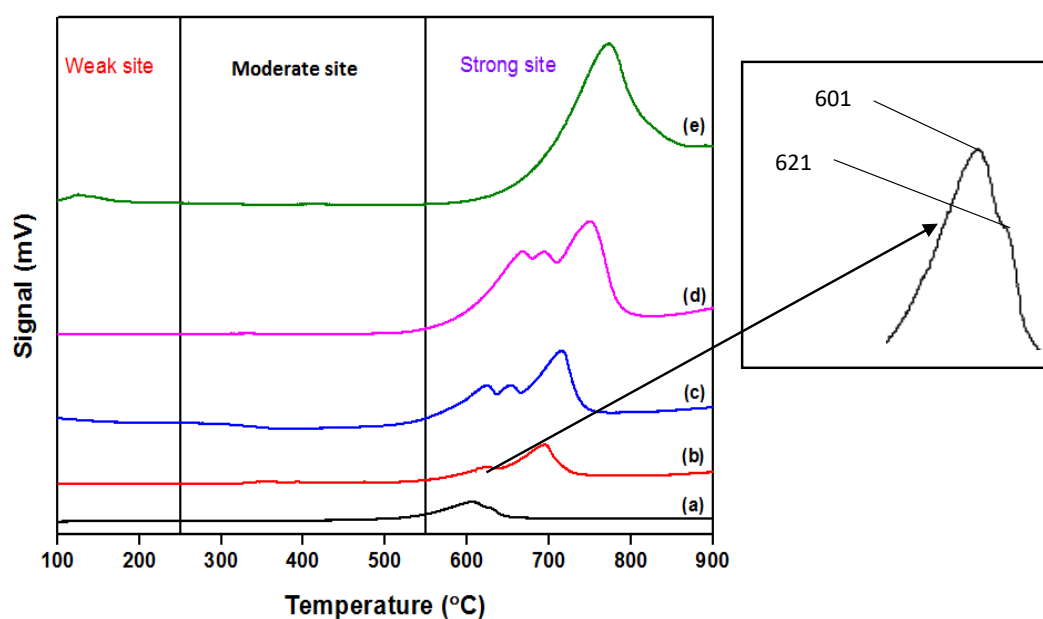


**Figure 6.** CO<sub>2</sub>-TPD profiles of (a) Dolomite (b) 5 wt% K/D (c) 10 wt% K/D (d) 15 wt% K/D (e) 20 wt% K/D.

**Table 2.** Total basicity of dolomite and various composition of K/D catalyst.

No.	Catalyst	Basic Site (μmol/g)	Temperature of CO <sub>2</sub> Desorption T <sub>max</sub> (°C)
1	Dolomite	501.4	601, 621
2	5K/D	892.2	603, 693
3	10K/D	1692.5	604, 648, 720
4	15K/D	3165.2	607, 683, 755
5	20K/D	1827.2	771

#### 2.4. Thermo Gravimetry–Differential Thermal Gravimetric (TG-DTG)

Figure 7a–e displays the TG-DTG curves of the dolomite and doped dolomite with different K<sub>2</sub>O contents. In general, the thermal behaviour of the compounds from room temperature to 1000 °C are similar. All DTG curves display an endothermic peak confirming the weight loss of the sample associated with the decomposition reaction for the compounds revealed in TG. The total mass loss for 20 wt% K/D, 15 wt% K/D, 10 wt% K/D, 5 wt% K/D and dolomite are 12 wt%, 47 wt%, 42 wt%, 77 wt% and 15 wt%, respectively, suggesting more thermal stability for the sample with higher K<sub>2</sub>O. The first thermal decomposition stage occurs in the range of 100–200 °C in all the samples, which is ascribed to loss of water. The second thermal decomposition stage occurs in the range 250–450 °C and is ascribed to the degradation of the dolomite structure with the release of CO<sub>2</sub> from the carbonate ion associated with the magnesium part of the structure. The decomposition is followed by the formation of calcite and magnesium oxide, as suggested by Equation (2).

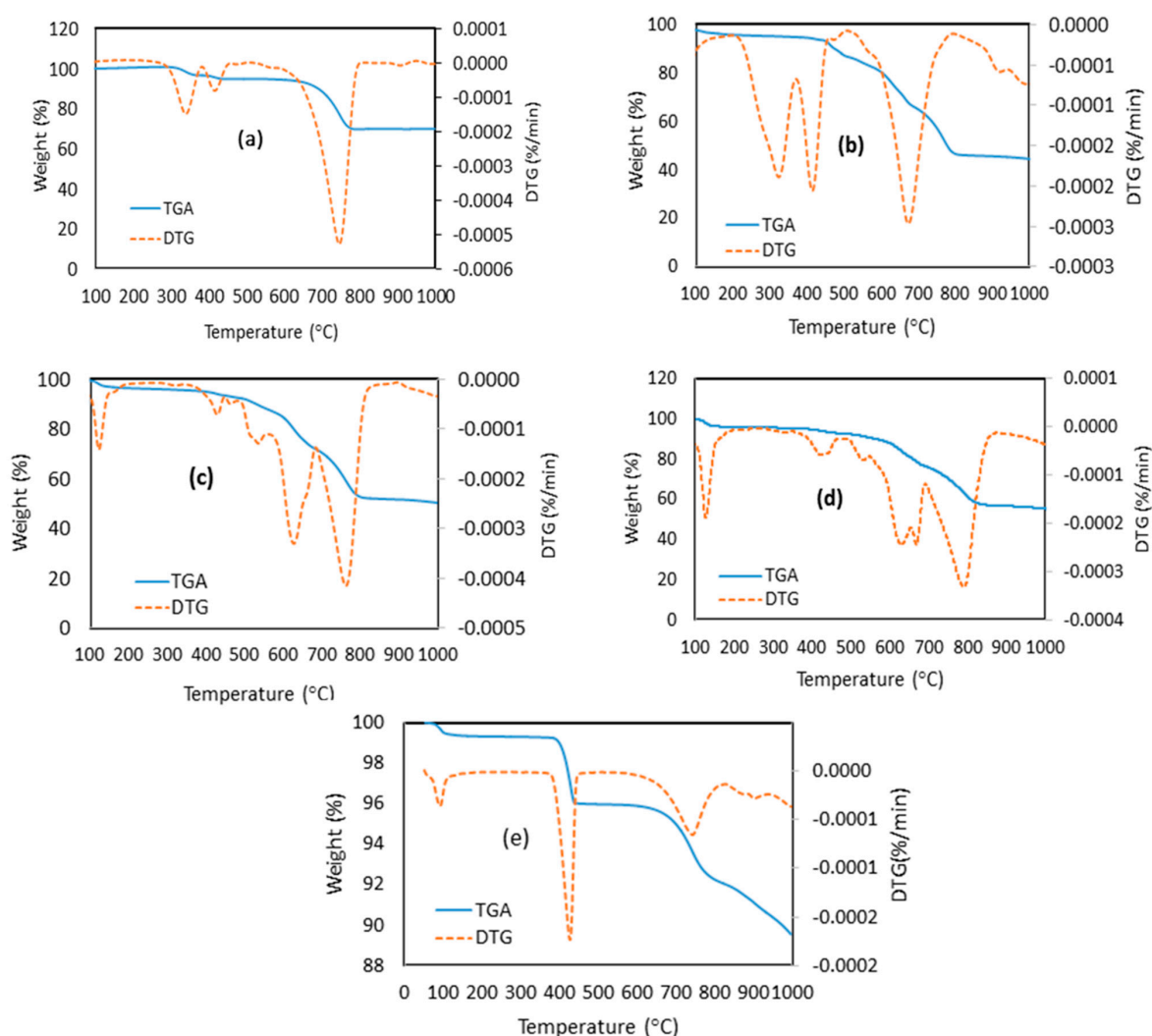


**Figure 7.** TGA-DTG thermogram of (a) Dolomite (b) 5 wt% K/D (c) 10 wt% K/D (d) 15 wt% K/D (e) 20 wt% K/D.

The peaks at higher temperature occurring in the range between 550–850 °C correspond to the degradation of calcite and potassium carbonate (doped dolomites) with the release of CO<sub>2</sub>, as ascribed by Equations (3) and (4), respectively.



This indicates that the decomposition of natural dolomite occurs in a stepwise manner to MgO and CaO, and does so when dolomite is doped with K<sub>2</sub>O. A subsequent XRD analysis of the dolomite and doped dolomite corroborated well with the TG-DTG analysis, which revealed peaks corresponding to MgO and CaO phases. According to [36], they reported that the decomposition temperatures of MgO and CaO were over 400 and 700 °C, respectively, which are similar to the result reported by [37]. These findings are similar to the decomposition temperatures obtained in this work.

### 2.5. Scanning Electron Microscope (SEM)

SEM images for dolomite and K<sub>2</sub>O/dolomite are presented in Figure 8. It was revealed that the dolomite is composed of an aggregation of homogeneous-sized particles of MgO and CaO which are segregated from each other. This is supported by XRD analysis, which showed the presence of these oxides. These segregated articles contribute to a high BET surface area (19.0 m<sup>2</sup>/g). When K<sub>2</sub>O was introduced on the dolomite, the micrograph showed a variation in surface morphology with the formation of a coarse particles in the case of 5 and 10 wt% K/D. The particles agglomerate into bigger ones as more K<sub>2</sub>O is added, as seen in 15 and 20 wt% K/D. Therefore, as the concentration of K<sub>2</sub>O on the support increases, the particle size increases which leads to the decrease in BET surface area, as seen in Table 1.

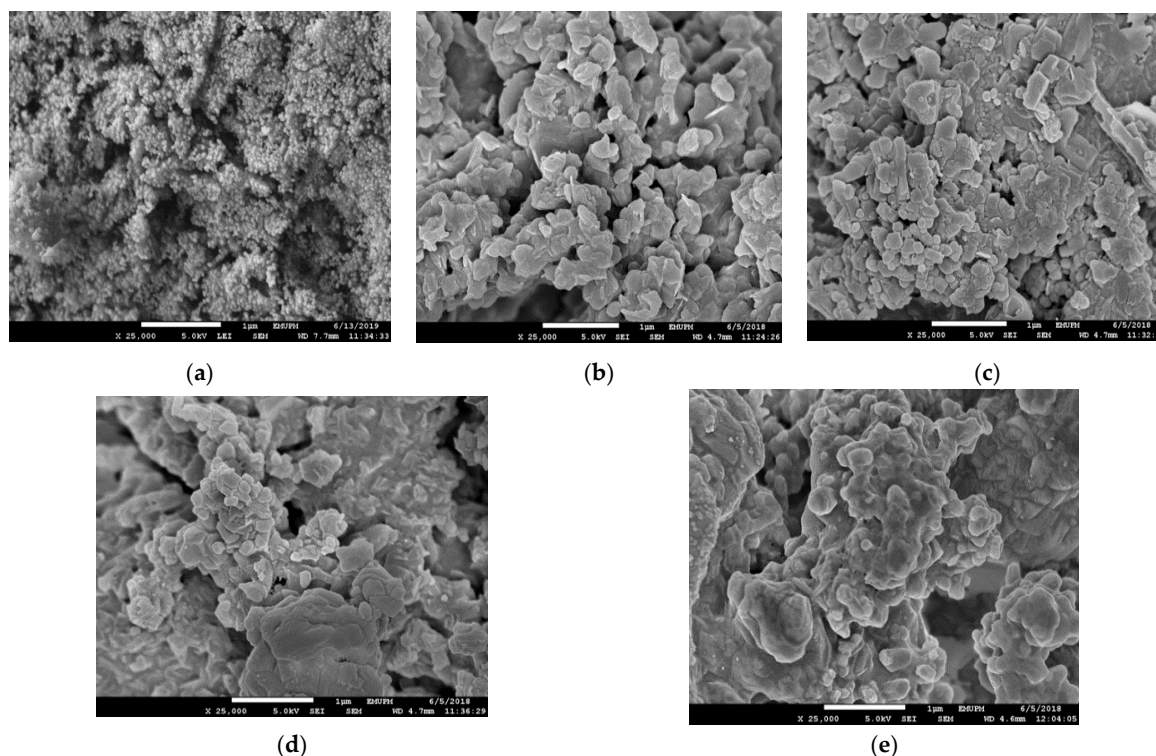


**Figure 8.** Surface morphology of (a) Dolomite (b) 5 wt% K/D (c) 10 wt% K/D (d) 15 wt% K/D (e) 20 wt% K/D.

## 2.6. Fourier Transform-Infrared Spectroscopy (FT-IR)

The FTIR spectrum of dolomite and  $K_2O$ -doped dolomite are depicted in Figure 9. The absorption band observed at 1433 and 866  $cm^{-1}$  in  $K_2O$ -doped dolomite catalysts are consistent with the observed band of the dolomite. These bands are attributed to the absorption band of Ca-O and Mg-O asymmetric stretching vibrations. Furthermore, the sharp peaks observed at 3691 and 3646  $cm^{-1}$  were attributed to  $OH^-$  group of  $Ca(OH)_2$  and  $Mg(OH)_2$ , respectively [38]. It was observed that the intensities of the bands decreased as the concentration of  $K_2O$  increased, with a little shift at all the peaks shown by the dolomite when aligned with  $K_2O$ -doped dolomite. This might be due to a decrease in the concentration of magnesium and calcium oxide by  $K_2O$ . The declaration of the aforementioned statement was confirmed by the XRD result.

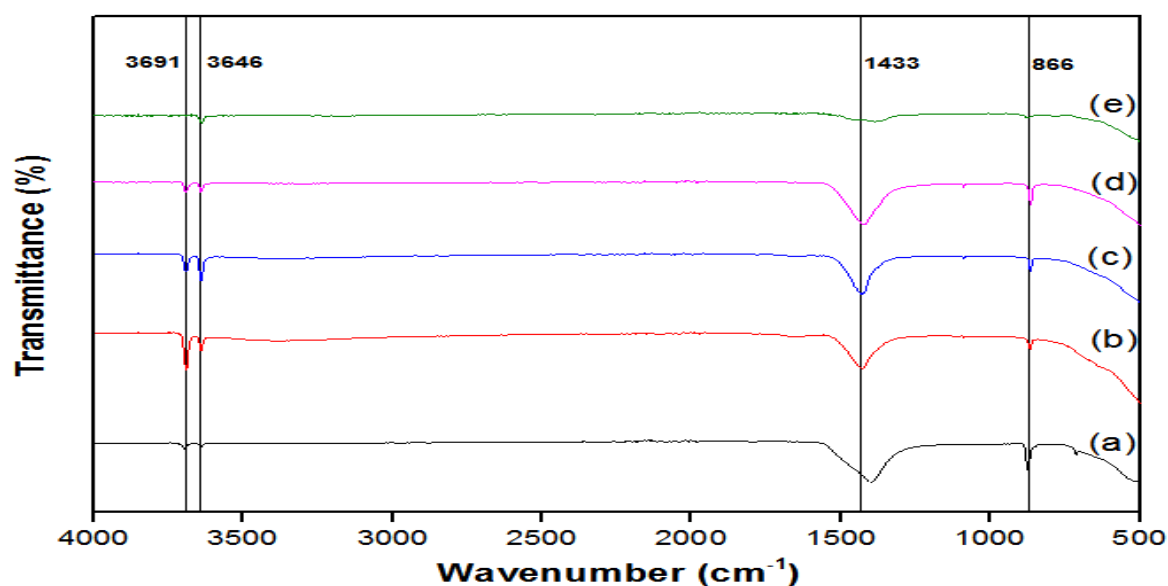
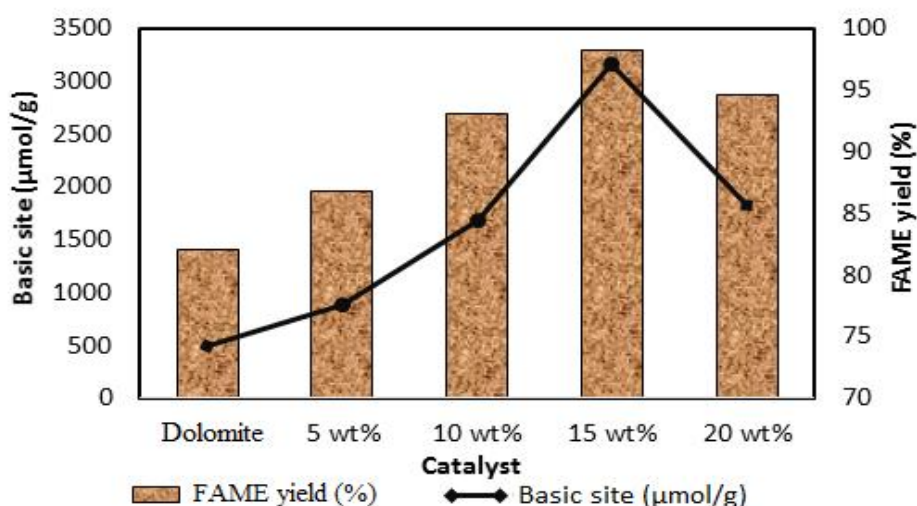


Figure 9. FTIR spectra of (a) Dolomite (b) 5 wt% K/D (c) 10 wt% K/D (d) 15 wt% K/D (e) 20 wt% K/D.

## 2.7. Catalytic Activity

The catalytic activity of the prepared catalyst was investigated in the transesterification reaction of palm oil at reaction conditions of 12:1 methanol to oil ratio, 1 wt% catalyst amount, a reaction temperature of 60 °C and 1 h reaction time. The catalytic activity of dolomite and doped dolomite was summarized in Figure 10. FAME yield was 87.3% over dolomite. When dolomite was doped with  $K_2O$ , the yield was increased as the amount of doped  $K_2O$  was increased. The maximum FAME yield of 98.7% was obtained by 15 wt% K/D. A declining yield was observed with further increases of dopant (20 wt% K/D). This could be due to the poor diffusion of the substrate when the catalyst was overloaded with dopant [17]. The catalytic activity of  $K_2O$ /dolomite showed a linear correlation to the basic site capacity. Therefore, the transesterification of palm oil to FAME over  $K_2O$ /dolomite is dependent on the function of basic site capacity, however, it was observed that the loading of  $K_2O$  beyond the optimum loading (15 wt%) reduces biodiesel yield as a result of K condensation caused by a lack of proper dispersion on the catalyst surface [39,40]. Thus,  $K_2O$  loading of 15 wt% was the optimum catalyst loading because it presented a significant catalytic activity in the reaction and produced the highest methyl ester of 98.7%.



**Figure 10.** Correlation between FAME yield, basic strength and catalyst loading.

### 2.8. Catalyst Reusability

The stability of the prepared potassium-oxide-doped dolomite catalyst was carried out by examining the number of reusability cycles. After the first reaction cycle, the catalyst was removed from the mixture by centrifugation. Later, the used catalyst was washed with methanol and hexane to remove the polar and non-polar compounds. The catalyst was applied for six consecutive experimental cycles under similar reaction conditions and the yield of each cycle is presented in Figure 11. The results showed that the catalyst can be reused for a successive four cycles with negligible loss in the catalytic activity with a FAME yield higher than 91.9%. The FAME yield in the subsequent cycles (5th and 6th) was less than 90%. The continuous decrease in FAME yield might be due to the leaching of potassium ion ( $\text{K}^+$ ) into the reaction solution. After the first cycle, the product was measured by Atomic Absorption Spectroscopy (AAS) to detect the leached  $\text{K}^+$  ion. After the fresh catalyst was used for the first cycle, it was found that the  $\text{K}^+$  leached into the product by having the highest value of 4.28 mg/L, as shown in Table 3. This could be due to the dopant in the fresh catalyst dissolved in the solvent and leached into the product. From the second cycle to the fourth cycle, the amount of  $\text{K}^+$  leached was decreasing linearly from 0.063 to 0.018 mg/L. It was then increased slightly from the fifth to sixth cycle (0.033 to 0.14 mg/L) which is reason for the decrease in FAME yield after the fifth and the sixth cycle.

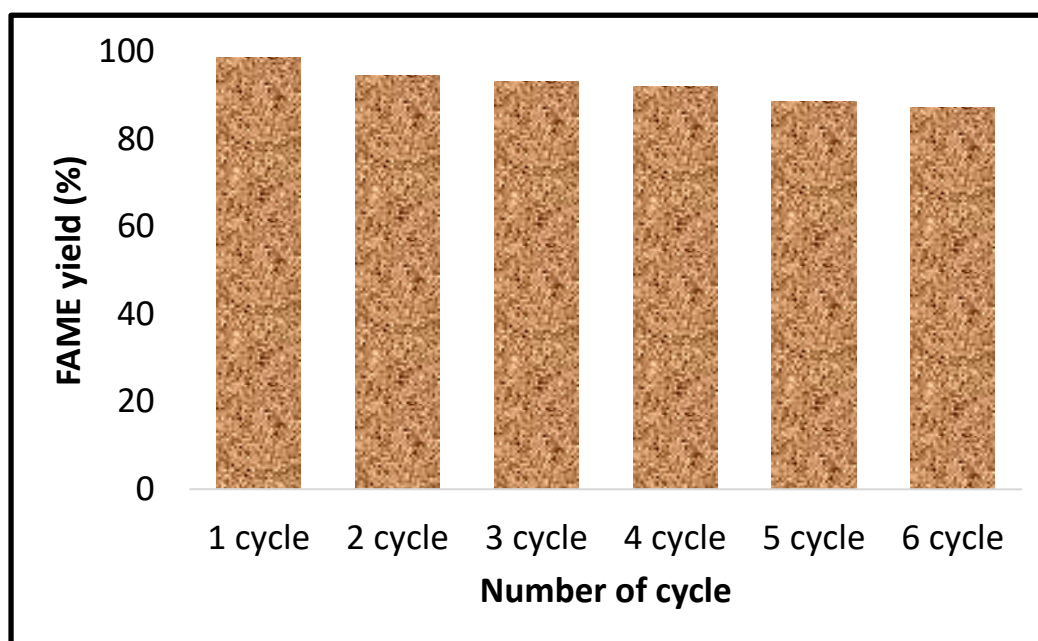


**Figure 11.** Reusability study of synthesized catalyst at optimized reaction condition (catalyst dosage 15 wt%, methanol to oil molar ratio 12:1, 60 °C reaction temperature and 1 wt% catalyst amount).

**Table 3.** Concentration of leached K<sup>+</sup> (mg/L) in different reusability samples by Atomic Absorption Spectroscopy (AAS).

S/N	FAME Yield	K <sup>+</sup> Concentration (mg/L)
1	98.7	4.82
2	94.4	0.063
3	93.1	0.025
4	91.9	0.018
5	88.6	0.033
6	87.2	0.14

### 2.9. Fuel Properties of Biodiesel

For the direct utilization of biodiesel in a diesel engine without adjustment, it has to meet the American society of testing and material (ASTM D6751) and European standards (EN 14214) specifications. The physicochemical properties of biodiesel produced from palm oil using the optimized catalyst of 15 wt% K/D are listed in Table 4 together with a comparison with ATSM D6751 and EN1412.

### 2.10. Viscosity

Viscosity is an essential property of fuel that affects the delivery and atomization of the fuel. It has been reported by the literature that the viscosity of synthesized methyl ester is greater than that of conventional diesel fuel by up to 1.6 times at a temperature of 40 °C [41]. Furthermore, higher or lower viscosity has an advanced effect on fuel engines. A higher viscosity affects the fuel flow rate at the time of intake stroke and also delays the fuel-air mixing process, while lower viscosity generates issues involving the exhaust emission caused as a result of incomplete combustion [42]. Hence, the viscosity of the biodiesel must conform to the American and European standard before utilization in fuel engines. In this work, the viscosity of the biodiesel produced from palm oil at 40 °C is 6.0, which was found to be on the borderline of the specified range of ASTM D6751 and slightly higher than the range specified by EN 14214.

**Table 4.** Fuel properties of biodiesel produced from palm oil compared with the ASTM biodiesel standard. [43].

Properties	Unit	ASTM D-6751	EN 14214	Biodiesel (This Work)
Kinematic viscosity	mm <sup>2</sup> /s at 40 °C	1.9–6.0	3.50–5.0	6.0
Saponification number	mg KOH/g	-	-	183.72
Mean molecular mass	g/mol	-	-	916.02
Acid value	mg KOH/g	≤0.05	<0.05	0.04
Density (15 °C)	(Kg/m <sup>2</sup> )	860–900	860–894	875
Pour point	(°C)	–15 to 9	-	5.0

### 2.11. Density

The density of biodiesel is higher than conventional diesel. The density of biodiesel fuel is affected by the degree of saturation and higher molecular weight of methyl ester. The density of biodiesel produced from palm oil was found to be 875 kg m<sup>-2</sup>, which conforms to both EN 14214 and ASTM D-6751 standards.

### 2.12. Pour Point

Pour point is among the essential parameters used to determine the quality of the fuel mixing and combustion process. It is the lowest temperature at which biodiesel has the ability to pour [30]. The synthesized biodiesel from palm oil presented a pour point at 5 °C which was found to be within the permissible limit of ASTM D-6751 standard with no specified standard of EN14124.

Table 5 exhibited the fatty acid composition of biodiesel produce from palm oil catalyzed by 15 wt% K/D. Among the fatty acid compositions of the synthesized biodiesel, Methyl oleate (18:2) presented the highest percentage of 46.56% *w/w*. Methyl palmitate is the next most abundant fatty acid after Methyl oleate with 39.70% *w/w*. Methyl stearate and Methyl linoleates are the 3rd and 4th most abundant fatty acids, with 8.46% and 3.11% *w/w*, respectively. Methyl myristate had the lowest mass fraction of 1.09% *w/w*. The results exhibited that the methyl ester composition of the synthesized biodiesel was 98.92% *w/w*, this indicated the successful conversion of palm oil to biodiesel.

**Table 5.** Fatty acid profile of biodiesel.

FAME	Structure	Composition (wt%)
Methyl myristate	C14:0	1.09
Methyl palmitate	C16:0	39.70
Methyl stearate	C18:0	8.46
Methyl oleate	C18:1	46.56
Methyl linoleates	C18:2	3.11

## 3. Materials and Methods

Dolomite was obtained in coarse aggregate forms from Northern Dolomite Sdn Bhd, Perlis, Malaysia. Palm oil was bought from a shopping mall in Seri Serdang, Selangor, Malaysia and K<sub>2</sub>CO<sub>3</sub> (99.5%) and CH<sub>3</sub>OH (99.8%) were all bought from R&M chemicals (Dhule, India).

### 3.1. Catalyst Preparation

The coarse aggregate of dolomite was ground and sieved to reduce its particle size to less than 24 µm. It was calcined in static air at 850 °C for 3 h to form calcined dolomite. For the potassium oxide (K<sub>2</sub>O)-doped dolomite catalysts, it was prepared by liquefying potassium carbonate (K<sub>2</sub>CO<sub>3</sub>) in distilled water and pouring 50 g of ground dolomite into the solution. For a 5 wt% K/D K<sub>2</sub>O loading, 3.6 g of K<sub>2</sub>CO<sub>3</sub> was dissolved in 50 mL of deionized water, while 10, 15 and 20 wt% K/D loadings require 7.3, 11.0 and 14.6 g of K<sub>2</sub>CO<sub>3</sub>, respectively. The solution was stirred for 90 min to ensure total

uniformity. The paste was later dried in an oven for 24 h at 110 °C and calcined in static air at 850 °C for 3 h using a vacuum furnace. The calcined catalyst was kept in an enclosed container to prevent moisture absorption. The catalyst was labelled as 5, 10, 15 and 20 wt% K/D.

### 3.2. Catalyst Characterization

The synthesized heterogeneous catalysts were analyzed by powder X-ray diffraction analysis using a Shimadzu diffractometer model XRD 6000 (Kyoto, Japan) at a scanning rate of 4°/min in the 2θ range of 20°–80°. The diffractometer employs Cu-Kα radiation to generate diffraction patterns from powder crystalline samples at room temperature with Philips glass diffraction X-ray tube broad focus 2.7 kW type. The specific surface area, pore volume and pore size distribution of the catalysts were studied by using a Brunauer–Emmett–Teller (BET) surface area analyzer with nitrogen adsorption at –196 °C. The basic strength of the catalysts was carried out using a temperature desorption program with CO<sub>2</sub> as a probe molecule (TPD-CO<sub>2</sub>). The samples (~0.05 g) were pre-treated by N<sub>2</sub> gas flow for 30 min at 300 °C. Then, the catalysts were subjected to CO<sub>2</sub> gas for an hour at room temperature to allow the adsorption of CO<sub>2</sub> onto the surfaces. Meanwhile, excess CO<sub>2</sub> was consequently flushed by N<sub>2</sub> gas. Desorption of the CO<sub>2</sub> from the basic sites of the samples was detected by TCD under helium gas flow (30 mL/min) from 50 to 900 °C and held for 30 min. Thermogravimetric analysis (TGA) was performed on a Mettler Toledo TG-SDTA apparatus to obtain the weight loss (TG) and derivative thermogravimetric (DTG) curves with the purge gas (nitrogen) flow rate of 30 mL min<sup>–1</sup> at the heating rate of 10 °C min<sup>–1</sup> from 25 to 1000 °C. The surface morphology of the catalysts was imaged by a JEOL scanning electron microscopy model JSM-6400. Very tiny particles of the catalyst were dispersed on a sample holder with double-sided tape and coated with a thin layer of gold by using BIO-RAS Sputter. The images were captured at different magnifications. The FTIR spectroscopy with a range of 4000–500 cm<sup>–1</sup> was used to study the functional groups present in catalyst samples using Shimadzu model FTIR-8300 (Kyoto, Japan). Catalyst samples were analyzed by spreading the samples in KBr and compressing the mixture to form discs.

### 3.3. Transesterification

The transesterification reaction was carried out in a batch-type reactor equipped with a thermocouple, magnetic stirrer, and reflux condenser. The flask was filled with 20 g of palm oil and at a methanol to oil ratio of 12:1 and then 1 wt% of catalyst at a reaction temperature of 60 °C for 1 h. The experiment was conducted at atmospheric pressure. The mixture was centrifuged for 15 min at 2000 rpm to separate the catalyst from the mixture. It was then heated at 65 °C (methanol boiling point) to remove excess methanol. The mixture was then transferred into separating funnel and stayed for 24 h to separate biodiesel from glycerol by gravity through the formation of two layers: the biodiesel at the upper layer and glycerol at the bottom layer. The remnants of the catalyst and other impurities were removed from the biodiesel layer by washing with warm water (50 °C) until the pH was 7 (neutral) (30). The number of methyl ester produced by transesterification reaction was investigated by gas chromatography flame ionization detector GC-FID (Agilent 7890A); the capillary column, length, thickness and internal diameter used were BP-20, 30 m, 0.5 mm and 0.25 μm respectively. The temperature of the oven was set at 150 °C and rose to 250 °C at a heating rate at 5 °C/min. The temperature for injector and detector were set at 250 and 280 °C, respectively. For the quantification of biodiesel yield, the internal standard used was methyl heptadecanoate. The yield was then calculated using the relation

$$\text{yield \%} = \frac{\text{weight of biodiesel} \times \% \text{FAME}}{\text{weight of oil}} \times 100$$

where %FAME is the concentration of FAME obtained from GC-FID, [2].

### 3.4. Reusability Study

The catalyst stability was studied under the following reaction conditions, which were 1 h reaction time, 60 °C temperature, 12:1 methanol to palm oil ratio, 15 w% catalyst load and 1 wt% of catalyst amount. After the first cycle of the experiment, the catalyst was removed from the product using centrifugation. The catalyst was further washed with methanol and subsequently with hexane to remove polar and non-polar compounds, respectively. It was then dried in an oven for 2 h at 110 °C and then used in the next reaction under similar conditions. The steps were repeated until the catalyst was reused for six cycles.

### 3.5. Leaching Test

The chemical stability of K<sub>2</sub>O-doped dolomite catalyst was determined by investigating the presence of free metal content in the biodiesel yield. This was done by Atomic Absorption Spectroscopy (AAS-S Series Thermo Scientific San Jose, CA, USA).

### 3.6. Biodiesel Assessment

The physicochemical properties of the biodiesel obtained from this work were examined according to the ASTM D6751 and EN 14214 of biodiesel standard. These properties include pour point, kinematic viscosity, density and acid value. The analysis was done at the Institute of Advanced Technology (ITMA) Universiti Putra Malaysia.

## 4. Conclusions

This study revealed that K<sub>2</sub>O/dolomite is a good catalyst with high activity in the transesterification of palm oil to produce biodiesel. The calcination of the catalyst was done at 850 °C for 3 h and evaluated for producing FAME. Under the reaction condition of temperature 60 °C, time 1 h, methanol to oil 12:1, catalyst amount 1 wt% and K<sub>2</sub>O loading of 15 wt% the FAME yield of 98.7% was attained. The catalyst was reused six times with the FAME yield higher than 90% in the four cycles. The produced biodiesel has fuel properties within ASTM and EN standards.

**Author Contributions:** Conceptualization, I.R. and N.S.I.; methodology, U.I.N.-U., N.S.I. and M.Y.; investigation, Y.H.T.-Y. and M.Y.; writing—original draft preparation, M.Y.; writing—review and editing, I.R. and M.Y.; supervision, Y.H.T.-Y. and E.N.M.; funding acquisition, I.R. All authors have read and agreed to the published version of the manuscript.

**Funding:** This research was funded by Universiti Putra Malaysia IPS grant number UPM's Putra Grant GP-IPS/2018/9619500.

**Acknowledgments:** The authors appreciate the financial support from the Universiti Putra Malaysia under IPS Grant, grant number 9619500. I also acknowledged the sponsorship received from Yobe State University, Nigeria.

**Conflicts of Interest:** The authors declare no conflict of interest.

## References

1. Boz, N.; Degirmenbasi, N.; Kalyon, D.M. Transesterification of canola oil to biodiesel using calcium bentonite functionalized with K compounds. *Appl. Catal. B Environ.* **2013**, *138–139*, 236–242. [[CrossRef](#)]
2. Chen, G.; Shan, R.; Shi, J.; Liu, C.; Yan, B. Biodiesel production from palm oil using active and stable K doped hydroxyapatite catalysts. *Energy Convers. Manag.* **2015**, *98*, 463–469. [[CrossRef](#)]
3. Yaakob, Z.; Mohammad, M.; Alherbawi, M.; Alam, Z.; Sopian, K. Overview of the production of biodiesel from Waste cooking oil. *Renew. Sustain. Energy Rev.* **2013**, *18*, 184–193. [[CrossRef](#)]
4. Ngamcharussrivichai, C.; Wiwatnimit, W.; Wangnoi, S. Modified dolomites as catalysts for palm kernel oil transesterification. *J. Mol. Catal. A Chem.* **2007**, *276*, 24–33. [[CrossRef](#)]
5. Farooq, M.; Ramli, A.; Subbarao, D. Biodiesel production from waste cooking oil using bifunctional heterogeneous solid catalysts. *J. Clean. Prod.* **2013**, *59*, 131–140. [[CrossRef](#)]

6. Ilgen, O.; Temp, R. Dolomite as a heterogeneous catalyst for transesterification of canola oil. *Fuel Process. Technol.* **2011**, *92*, 452–455. [[CrossRef](#)]
7. Wang, S.; Zhao, C.; Shan, R.; Wang, Y.; Yuan, H. A novel peat biochar supported catalyst for the transesterification reaction. *Energy Convers. Manag.* **2017**, *139*, 89–96. [[CrossRef](#)]
8. Marques, L.; de Sousa, N.; Sousa, D.; Loureiro, C., Jr.; Antonio, J.; Rodríguez-castellón, E.; Silveira, R. Characterization and application of dolomite as catalytic precursor for canola and sunflower oils for biodiesel production. *Chem. Eng. J.* **2015**, *269*, 35–43. [[CrossRef](#)]
9. Sharma, Y.C.; Singh, B. Development of biodiesel: Current scenario. *Renew. Sustain. Energy Rev.* **2009**, *13*, 1646–1651. [[CrossRef](#)]
10. Baskar, G.; Aiswarya, R. Trends in catalytic production of biodiesel from various feedstocks. *Renew. Sustain. Energy Rev.* **2016**, *57*, 496–504. [[CrossRef](#)]
11. Chen, G.; Shan, R.; Yan, B.; Shi, J.; Li, S.; Liu, C. Remarkably enhancing the biodiesel yield from palm oil upon abalone shell-derived CaO catalysts treated by ethanol. *Fuel Process. Technol.* **2016**, *143*, 110–117. [[CrossRef](#)]
12. Peterson, G.R.; Scarrah, W.P. Rapeseed Oil Transesterification by Heterogeneous Catalysis. *J. Am. Oil Chem. Soc.* **1984**, *61*, 1593–1594. [[CrossRef](#)]
13. Kataria, J.; Mohapatra, S.K.; Kundu, K. Biodiesel production from waste cooking oil using heterogeneous catalysts and its operational characteristics on variable compression ratio CI engine. *J. Energy Inst.* **2018**, *1*–13. [[CrossRef](#)]
14. Avhad, M.R.; Marchetti, J.M. A review on recent advancement in catalytic materials for biodiesel production. *Renew. Sustain. Energy Rev.* **2015**, *50*, 696–718. [[CrossRef](#)]
15. Samart, C.; Chaiya, C.; Reubroycharoen, P. Biodiesel production by methanolysis of soybean oil using calcium supported on mesoporous silica catalyst. *Energy Convers. Manag.* **2010**, *51*, 1428–1431. [[CrossRef](#)]
16. Zabeti, M.; Mohd, W.; Wan, A.; Aroua, M.K. Activity of solid catalysts for biodiesel production: A review. *Fuel Process. Technol.* **2009**, *90*, 770–777. [[CrossRef](#)]
17. Sun, C.; Qiu, F.; Yang, D.; Ye, B. Preparation of biodiesel from soybean oil catalyzed by Al-Ca hydrotalcite loaded with K<sub>2</sub>CO<sub>3</sub> as heterogeneous solid base catalyst. *Fuel Process. Technol.* **2014**, *126*, 383–391. [[CrossRef](#)]
18. Shan, R.; Shi, J.; Yan, B.; Chen, G.; Yao, J.; Liu, C. Transesterification of palm oil to fatty acids methyl ester using K<sub>2</sub>CO<sub>3</sub>/palygorskite catalyst. *Energy Convers. Manag.* **2016**, *116*, 142–149. [[CrossRef](#)]
19. Aslan, S.; Aka, N.; Karaoglu, M.H. Environmental Effects NaOH impregnated sepiolite based heterogeneous catalyst and its utilization for the production of biodiesel from canola oil. *Energy Sources Part A Recover. Util. Environ. Eff.* **2018**, *1*–8. [[CrossRef](#)]
20. Nur, Z.A.S.; Taufiq-Yap, Y.H.; Hussein, M.Z. Tin Oxide Doped on Activated Dolomites as Efficient Catalyst for Biodiesel Production. *Adv. Mater. Res.* **2012**, *620*, 378–383. [[CrossRef](#)]
21. Jindapon, W.; Ngamcharussrivichai, C. Heterogeneously catalyzed transesterification of palm oil with methanol to produce biodiesel over calcined dolomite: The role of magnesium oxide. *Energy Convers. Manag.* **2018**, *171*, 1311–1321. [[CrossRef](#)]
22. Buasri, A.; Rochanakit, K.; Wongvitvichot, W. The Application of Calcium Oxide and Magnesium Oxide from Natural Dolomitic Rock for Biodiesel Synthesis. *Energy Procedia* **2015**, *79*, 562–566. [[CrossRef](#)]
23. Maes, I.I.; Gryglewicz, G.; Yperman, J.; Franco, D.V.; Van Poucke, L.C. Effect of calcium and calcium minerals in coal on its thermal analysis. *Fuel* **1997**, *76*, 143–147. [[CrossRef](#)]
24. Patnaik, P.; York, N.; San, C.; Lisbon, F.; Madrid, L.; City, M.; New, M.; San, D.; Singapore, J.S.; Toronto, S. *Handbook of Inorganic Chemicals. McGraw-Hill Library of Congress Cataloging-in-Publication Data*; McGraw-Hill: New York, NY, USA, 2003; ISBN 0-07-049439-8.
25. Wilson, K.; Hardacre, C.; Lee, A.F.; Montero, M.; Shellard, L. The application of calcined natural dolomitic rock as a solid base catalyst in triglyceride transesterification for biodiesel synthesis. *Green Chem.* **2008**, *10*, 654–659. [[CrossRef](#)]
26. Wang, L.; Yang, J. Transesterification of soybean oil with nano-MgO or not in supercritical and subcritical methanol. *Fuel* **2007**, *86*, 328–333. [[CrossRef](#)]
27. Xie, W.; Li, H. Alumina-supported potassium iodide as a heterogeneous catalyst for biodiesel production from soybean oil. *J. Mol. Catal. A Chem.* **2006**, *255*, 1–9. [[CrossRef](#)]
28. Krstic, J.; Jovanovic, D. Alumina/silica supported K<sub>2</sub>CO<sub>3</sub> as a catalyst for biodiesel synthesis from sunflower oil. *Bioresour. Technol.* **2009**, *100*, 4690–4696. [[CrossRef](#)]

29. Liu, H.; Su, L.; Liu, F.; Li, C.; Solomon, U.U. Cinder supported  $K_2CO_3$  as catalyst for biodiesel production. *Appl. Catal. B Environ.* **2011**, *106*, 550–558. [[CrossRef](#)]
30. Issariyakul, T.; Dalai, A.K. Biodiesel from vegetable oils. *Renew. Sustain. Energy Rev.* **2014**, *31*, 446–471. [[CrossRef](#)]
31. Pure, U.O.F. Provisional International Union of Pure and Applied Chemistry Commission on Colloid and Surface Chemistry Subcommittee on Reporting Gas Adsorption Data \* Reporting Physisorption Data for Gas/Solid Systems with Special Reference to the Determination of S. *Pure Appl. Chem.* **1982**, *54*, 2201–2218.
32. Noiroj, K.; Intarapong, P.; Luengnaruemitchai, A.; Jai-in, S. A comparative study of KOH/ $Al_2O_3$  and KOH/NaY catalysts for biodiesel production via transesterification from palm oil. *Renew. Energy* **2009**, *34*, 1145–1150. [[CrossRef](#)]
33. Limmanee, S.; Naree, T.; Bunyakiat, K.; Ngamcharussrivichai, C. Mixed oxides of Ca, Mg and Zn as heterogeneous base catalysts for the synthesis of palm kernel oil methyl esters. *Chem. Eng. J.* **2013**, *225*, 616–624. [[CrossRef](#)]
34. Yan, S.; Dimaggio, C.; Mohan, S.; Kim, M.; Salley, S.O.; Ng, K.Y.S. Advancements in Heterogeneous Catalysis for Biodiesel Synthesis. *Top. Catal.* **2010**, *53*, 721–736. [[CrossRef](#)]
35. Taufiq-Yap, Y.H.; Lee, H.V.; Hussein, M.Z.; Yunus, R. Calcium-based mixed oxide catalysts for methanolysis of *Jatropha curcas* oil to biodiesel. *Biomass Bioenergy* **2011**, *35*, 827–834. [[CrossRef](#)]
36. Mcintosh, R.M.; Sharp, J.H.; Wilburn, F.W. The thermal decomposition of dolomite. *Thermochim. Acta* **1990**, *165*, 281–296.
37. Olszak-Humienik, M.; Jablonski, M. Thermal behavior of natural dolomite. *J. Therm. Anal. Calorim.* **2015**, *119*, 2239–2248. [[CrossRef](#)]
38. Zhang, H.; Yang, H.; Guo, H.; Yang, J.; Xiong, L.; Huang, C.; Chen, X.; Ma, L.; Chen, Y. Solvent-free selective epoxidation of soybean oil catalyzed by peroxophosphotungstate supported on palygorskite. *Appl. Clay Sci.* **2014**, *90*, 175–180. [[CrossRef](#)]
39. Wang, S.; Yuan, H.; Wang, Y.; Shan, R. Transesterification of vegetable oil on low cost and efficient meat and bone meal biochar catalysts. *Energy Convers. Manag.* **2017**, *150*, 214–221. [[CrossRef](#)]
40. Zhao, C.; Yang, L.; Xing, S.; Luo, W.; Wang, Z.; Lv, P. Biodiesel production by a highly effective renewable catalyst from pyrolytic rice husk. *J. Clean. Prod.* **2018**, *199*, 772–780. [[CrossRef](#)]
41. Tesfa, B.; Mishra, R.; Gu, F.; Powles, N. Prediction models for density and viscosity of biodiesel and their effects on fuel supply system in CI engines. *Renew. Energy* **2010**, *35*, 2752–2760. [[CrossRef](#)]
42. Zaharin, M.S.M.; Abdullah, N.R.; Naja, G.; Sharudin, H.; Yusaf, T. Effects of physicochemical properties of biodiesel fuel blends with alcohol on diesel engine performance and exhaust emissions: A review. *Renew. Sustain.* **2017**, *79*, 475–493. [[CrossRef](#)]
43. Sarin, A.; Arora, R.; Singh, N.P.; Sarin, R.; Malhotra, R.K. Blends of biodiesels synthesized from non-edible and edible oils: Influence on the OS (oxidation stability). *Energy* **2010**, *35*, 3449–3453. [[CrossRef](#)]

